Impaired Cortico-Amygdala Functional Connectivity Can Drive Social Behavior Deficits in Synucleinopathies

Wei Zhou[1], Samuel Daniels[1,2], Vijay Singh[4], Marissa Menard[4,5], Martha L Escobar Galvis[3], Hong-Yuan Chu[1,5,*]

1 Department of Neurodegenerative Science, Van Andel Research Institute, Grand Rapids, MI 49503, USA

2 Van Andel Institute Graduate School, Grand Rapids, MI, 49503, USA

3 Core Technologies and Services Van Andel Institute, Grand Rapids, MI 49503, USA

4 Center for Neurodegeneration and Experimental Therapeutics, University of Alabama at Birmingham, Birmingham, Alabama 35294, USA

5 Aligning Science Across Parkinson's (ASAP) Collaborative Research Network, Chevy Chase, MD, 20852, United States

*Corresponding author: Hong-Yuan Chu, Ph.D.; Email: hc948@georgetown.edu

18 **Declarations**

19 **Ethics approval.** Animal studies were reviewed and approved by the Institutional Animal Care
20 and Use Committee at Van Andel Institute (animal use protocol #: 22-02-007) and in accordance
21 with the standards of NIH for care and use of animals.

22 **Availability of data and materials**. The datasets used and/or analyzed during the current study
23 are available from the corresponding author on reasonable request.

24 **Competing interests**. The authors declare that they have no competing interests.

25 **Funding**. This work was partially supported by research grants from Brain and Behavior
26 Research Foundation (grant#: 29037, H.Y.C.), Department of Defense Congressionally Directed
27 Medical Research Programs (grant#: W81XWH-21-1-0943, H.Y.C.). This work was also funded in
28 whole or in part by Aligning Science Across Parkinson's (ASAP-020572) through the Michael J.
29 Fox Foundation for Parkinson's Research (MJFF) and Aligning Science Across Parkinson's
30 Disease-PFF support and characterization (ASAP-022091) through the Michael J Fox Foundation
31 for Parkinson's Research to LVD. For the purpose of open access, the authors have applied a CC
32 BY public copyright license to all Author Accepted Manuscripts arising from this submission.

33 **Authors' contributions**. WZ conducted stereotaxic surgeries, electrophysiological recordings,
34 and behavioral tests, analyzed data and interpreted results, and wrote initial draft. SD
35 conducted stereotaxic surgeries and behavioral tests. VS and MM generated and validated
36 mouse α-synuclein preformed fibrils and wrote the initial draft. MEG contributed to acquisition
37 of grant supports, interpreting results, as well as writing and editing the manuscript. HYC
38 contributed to conceptualization of the project, obtaining of grant supports and the

administration, as well as analyzing and interpreting data, writing, editing and revising the manuscript. All authors read and approved the final manuscript.

Acknowledgement. The authors thank Van Andel Institute vivarium technician team for animal husbandry, and Ms. Rachel Dvorak for initial technical assistance in animal surgery. The authors thank Dr. Qiang Zhu at Van Andel Institute for general support in grant administration.

Authors' information. The current affiliation of ZW and HYC is Department of Pharmacology and Physiology, Georgetown University Medical Center, Washington D.C., 20007, USA

Abstract

The small molecule protein α-synuclein forms insoluble aggregates in a group of neurological disorders, including Parkinson's disease and dementia with Lewy bodies, that are collectively called synucleinopathies. However, it remains poorly understood how the aggregated α-synuclein disrupts normal connectivity and function of complex neural circuits, prior to robust neurodegeneration, leading to the manifestation of various motor, emotion, and cognitive symptoms in synucleinopathies. In the present study, we combined electrophysiology, optogenetics, mouse model of synucleinopathies, and behavioral analysis to address this question. Using an α-synuclein preformed fibrils-based mouse model of synucleinopathies, we reported dynamic changes in the levels of α-synuclein pathology in the basolateral amygdala (BLA) circuits. Such dynamic changes associated with an accumulation of α-synuclein aggregates within cortical glutamatergic afferents to the BLA at an initial stage, followed by gradual loss of cortical inputs and BLA principal neurons at late stage. Moreover, we found that the cortical, but not the thalamic, afferents to the BLA showed functional impairments that were highly correlated with the manifestation of defected sociability in mice with α-synuclein pathology. Furthermore, we provided experimental evidence showing that the impaired social behavior of mice was rescued by chemogenetic stimulation of cortico-BLA inputs. Altogether, we presented a series of evidence to delineate key circuit events associated with α-synuclein pathology development in a complex neuronal network. The present work highlights the necessity of a thorough investigation of functional consequences of α-synuclein aggregation to advance our understand of pathophysiology of synucleinopathies and development of effective therapies.

Keywords

α-synuclein, synucleinopathies, Parkinson's disease, medial prefrontal cortex, amygdala, electrophysiology, optogenetics, neural circuit, synapse, sociability

Background

Abnormally folded and aggregated α-synuclein (α-Syn) is the major proteinaceous component of the intraneuronal inclusions that characterize Lewy pathology [1, 2]. Lewy pathology can be found in most brains of people with Parkinson's disease (PD), dementia with Lewy bodies (DLB), and multiple system atrophy. These disorders are collectively known as "synucleinopathies" [2]. Experimental work suggests that gradual accumulation of α-Syn aggregates can underlie the pathogenesis and progression of synucleinopathies [3-5]. Particularly, accumulation of pathologic α-Syn in the dopaminergic neurons of the substantia nigra pars compacta (SNc) and their axons has been reported to impair nigrostriatal dopaminergic neurotransmission and perhaps underlie the neurodegeneration, which eventually results in the manifestation of motor symptoms in PD [4, 6, 7]. In addition, α-Syn pathology is proposed to spread between cells and brain regions [3, 5, 8, 9]. Consequently, a large body of studies have focused on understanding the genetic and microenvironmental factors that may promote or prevent the formation of pathologic α-Syn aggregation, as they perhaps can provide us with strategies to regulate the temporal development and spatial distribution of α-Syn pathology across brain regions and in that way modify disease progression [10-15].

Over the progression of diseases over decades, deposition of α-Syn aggregates in the brain is not the end stage of the disease and the subsequent degeneration of vulnerable neuronal populations is just one of the biological events associated with synucleinopathies. It has been shown that a threshold of SNc dopaminergic neurodegeneration needs to be reached prior to the manifestation of motor deficits both in PD and its animal models [16, 17], which might related to the development of an abnormal brain network activity following a severe

96 dopamine depletion [18, 19]. Consistently, compelling evidence also suggests that α-Syn
97 aggregates disrupt synaptic structure, function, and plasticity in susceptible brain regions [4, 20-
98 22].

99 In the context of complex neural circuits, many other factors must be considered to
100 better understand how α-Syn pathology impairs normal circuitry function. First, not all brain
101 regions and cell subtypes express equal levels of endogenous α-Syn, and therefore should not
102 have the same vulnerability to α-Syn aggregation [23-27]. Second, the brain network is
103 equipped with a battery of neural plasticity mechanisms that counteract circuit perturbations
104 [28]. Therefore, as α-Syn aggregates accumulate in a complex brain network, it is plausible to
105 hypothesize that 1) synaptic function and cellular activity of vulnerable cells are impaired at
106 early stage, prior to overt neurodegeneration; 2) neural network activity is altered by both the
107 direct detrimental effects of α-Syn aggregation and the associated compensatory adaptions;
108 and/or 3) early signs of behavioral deficits are more closely associated with the impaired circuit
109 function by α-Syn pathology, rather than with neurodegeneration itself.

110 To test the above hypotheses, we interrogated the basolateral amygdala (BLA)
111 microcircuits while α-Syn pathology progressively developed over an extended period of time.
112 We chose to use the BLA microcircuit as a model system because the amygdala is a hotspot for
113 Lewy pathology development in both PD and DLB [29-32] and its circuitry dysfunction has been
114 linked to emotional dysregulation in humans [33-36]. Anatomically, the BLA receives both
115 cortical and thalamic synaptic inputs, which exhibit distinct vulnerability to α-Syn pathology
116 [26]. Thus, α-Syn aggregation is likely to disrupt normal emotion encoding by the amygdala
117 microcircuits through a series of sequential events. Our work here provides novel insights into

118 how α-Syn pathology can disrupt information processing in a complex network and thereafter

119 contributes to the development of behavioral deficits. Altogether, our findings contribute to our

120 understanding of circuit events associated with α-Syn aggregation in complex microcircuits.

121

122 **Materials and methods**

123 **Animals**

124 C57BL/6J mice at 2-3-month-old (Jax#:000664, RRID: IMSR_JAX:000664) of both sexes were
125 obtained through the Van Andel Institute vivarium and used in this study. All animal studies
126 were reviewed and approved by the Institutional Animal Care and Use Committee at Van Andel
127 Institute (animal use protocol #: 22-02-007) and in accordance with the standards of NIH for
128 care and use of animals. Animals were housed under a 12:12 h light-dark cycle, up to four
129 animals per cage with access to water and food *ad libitum*.

130

131 **Preparation and validation of α-Syn preformed fibrils**

132 The mouse α-Syn protein was purified using *Escherichia coli* BL21 codon plus RIPL cells, which
133 was then dialyzed using a buffer containing 10 mM Tris and 50 mM NaCl (pH 7.5). A high-
134 capacity endotoxin removal kit (PI88276) was used to remove the endotoxins, the levels of
135 which were assessed using an endotoxin quantification kit (A39552). The protein concentration
136 was estimated using absorbance at 280 nm with an extinction coefficient of 7450 M^{-1} cm^{-1}.
137 Purified mouse α-Syn monomer protein was used to generate mouse α-Syn preformed fibrils
138 (PFFs). Specifically, monomeric α-Syn protein was diluted to 5 mg/mL in the buffer, 150 mM KCl,
139 50 mM Tris-HCl and incubated at 37°C with shaking for 7 days, as described previously [37]. After
140 the incubation, sample was centrifuged for 10 min at 13,200 rpm. The protein pellet was re-
141 suspended in half of the initial volume of the solution. To estimate the fibril concentration, 5 µl
142 of fibril solution was incubated with 5 µL of 8 M guanidinium chloride at room temperature for
143 one hour. After incubation, the concentration of PFF was measured using absorbance at 280 nm

144 and diluted the PFF at 5 mg/mL and 22-25 µl aliquots were stored at −80°C until use. Prior to
145 the injection, PFF aliquot (22-25 µl at 5 mg/mL) was thawed at room temperature and sonicated
146 using Qsonica 700W cup horn sonicator at 30% amplitude using 3 seconds on/2 seconds off
147 cycle for 15 min at 15°C. The size of sonicated PFF (30-70 nm segments) was estimated and
148 confirmed using the dynamic light scattering (DynaPro NanoStar from Wyatt technology).
149

150 **Stereotaxic surgery**

151 Motorized stereotaxic frames were used for stereotaxic injections (Model# 51730M, Stoelting
152 Co.). Mice were anesthetized with 2% isoflurane and placed on a heating pad throughout the
153 surgery for maintenance of the body temperature. Eye ointment was administered to keep eyes
154 moisture and to protect them from strong light. To induce α-Syn pathology in mouse brain, we
155 bilaterally injected the sonicated PFFs (10 µg in a 2.0 µL volume) into the dorsal striatum
156 (anteroposterior (A-P), +0.2 mm from bregma; mediolateral (M-L), ± 2.0 mm from the midline;
157 dorsoventral (D-V), -2.9 mm from the brain surface) using a Nanoliter injector (NANOLITER2020,
158 World Precision Instrument) at a rate of 0.4 µL/min. To label the BLA principal neurons for
159 electrophysiological recordings, Retrobeads (LumaFluor Inc) were diluted (1:10 dilution) into
160 PFFs or PBS and then the mixed materials were co-injected into the dorsal striatum. Mice
161 injected with PBS or PBS plus beads at the same age were made as control groups. To
162 optogenetically evoke excitatory postsynaptic currents (EPSCs) of BLA projection neurons, we
163 injected 0.3 µL AAVs encoding ChR2(H134R)-eYFP (titer = 1 x 10^{12} GC/ml, Addgene# 26973,
164 RRID: Addgene_127090) into the layer 5 of medial prefrontal cortex (mPFC, A-P, +2.1 mm from
165 bregma; M-L, ± 0.3 mm from the midline; D-V, -2.3 mm from the brain surface) and the

166 centromedial thalamus (A-P, -1.5 mm from bregma; M-L, 0 mm from the middle; D-V, -3.3 mm
167 from the brain surface) at a rate of 0.1 µL/min. An intersectional approach was used for
168 selective activation of mPFC to BLA projection using chemogenetics: 1) retrograde AAV encoding
169 FlpO (0.3 µL, titer ≥ 7 x 10^{12} GC/ml, Addgene# 55637) were bilaterally injected into BLA (A-P, -1.3
170 mm from bregma; M-L, ± 3.3 mm from the middle; D-V, -4.4 mm from the brain surface), and 2)
171 AAVs encoding FlpO-dependent excitatory designer receptors exclusively activated by designer
172 drugs (DREADDs) (titer = 2.5 x 10^{13} GC/ml, Addgene 154868) were injected into infralimbic
173 subregion of mPFC (IL-mPFC) (A-P, +2.1 mm from bregma; M-L, ± 0.3 mm from the midline; D-V,
174 -2.6 mm from the brain surface). Animals were returned to a cage placed on a warm pad after
175 surgery and then housed in their home cage until experiments. Details of this protocol can be
176 found at: https://doi.org/10.17504/protocols.io.rm7vzye28l×1/v1.
177

178 **Slice preparation for *ex vivo* physiological recording**

179 To prepare brain slices for physiological recording, mice were intraperitoneally injected with
180 avertin (300 mg/kg) for anesthesia, followed by transcardial perfusion using ice-cold, sucrose-
181 based artificial cerebrospinal fluid (aCSF), containing the follows (in mM): 230 sucrose, 26
182 $NaHCO_3$, 10 glucose, 10 $MgSO_4$, 2.5 KCl, 1.25 NaH_2PO_4, 0.5 $CaCl_2$, 1 sodium pyruvate, and 0.005
183 L-glutathione. Brain slices (300 µm thickness) with the BLA were collected using a vibratome
184 (VT1200S; Leica Microsystems, Buffalo Grove, IL) in the same sucrose-aCSF. Throughout the
185 preparation, brain slices were kept at about +4°C by a recirculating chiller (FL300; JULABO USA,
186 Inc, Allentown, PA). Then the slices were incubated at 35°C in regular aCSF bubbled with 95% O_2
187 and 5% CO_2 for 30 min (in mM, 126 NaCl, 26 $NaHCO_3$, 10 glucose, 2.5 KCl, 2 $CaCl_2$, 2 $MgSO_4$, 1.25

188 NaH_2PO_4, 1 sodium pyruvate, and 0.005 L-glutathione), and then kept at room temperature for
189 at least another 30 min prior to recording.
190
191 **Slice electrophysiology recording and optogenetics**
192 Brain slices were transferred to recording chamber with modified aCSF (in mM, 126 NaCl, 26
193 NaHCO3,10 glucose, 3 KCl, 1.6 $CaCl_2$,1.5 $MgSO_4$, and 1.25 NaH_2PO_4), which was equilibrated
194 with 95% O_2 and 5% CO_2 at 32–34°C via a feedback-controlled in-line heater (TC-324C, Warner
195 Instruments). A gradient contrast SliceScope 1000 (Scientifica, UK) with an IR-2000 CCD camera
196 (DAGE-MTI, USA) using infrared illumination was used to visualize neurons in slices. A motorized
197 micromanipulator was used to control the position of the glass pipette for recording. The BLA
198 principal cells were identified based on the presence of somatic Retrobeads signals under a 60x
199 water immersion object lens (Olympus, Japan).
200 Electrophysiology data were collected using an Axon 700B amplifier and digitized with a
201 1550B digitizer (Molecular Devices, San Jose, USA). Signals were low pass filtered at 2 kHz and
202 sampled at 50 kHz under the control of pClamp 11 (RRID: SCR_011323, Molecular Devices, San
203 Jose, USA). Borosilicate glass pipettes with resistance at 4-6 MΩ (O.D. = 1.5 mm, I.D. = 0.86, item
204 # BF150-86-10, Sutter Instruments, Novato, CA) were made by a micropipette puller (P1000,
205 Sutter Instruments, Novato, CA). For voltage-clamp recordings of synaptic transmission, a Cs^+-
206 based intracellular solution containing the following (in mM): 120 CH_3O_3SCs, 2.8 NaCl, 10 HEPES,
207 0.4 Na_4-EGTA, 5 QX314-HBr, 5 phosphocreatine, 0.1 spermine, 4 ATP-Mg, and 0.4 GTP-Na was
208 used; the pH was adjusted to pH 7.3 with CsOH. A K-gluconate-based internal solution (in mM,
209 140 K-gluconate, 3.8 NaCl, 1 MgCl2, 10 HEPES, 0.1 Na_4-EGTA, 2 ATP-Mg, and 0.1 GTP-Na, 0.2%

210 Biocytin, pH 7.3, 290 mOsm) was used to label the BLA projections neurons for morphology
211 studies using Cy-streptavidin. For optogenetic stimulation, light pulses with 1 ms duration were
212 delivered through a 60x objective lens (Olympus, Japan) using a 470 nm LED light illumination
213 (CoolLED, UK). TTX (1 µM) and 4-AP (100 µM) were perfused to isolate monosynaptic mPFC-BLA
214 neurotransmission. To measure the synaptic strength, peak amplitude of AMPARs-mediated
215 EPSCs at -80 mV were calculated. Paired-pulse ratio at 10 Hz was quantified as the ratio of
216 amplitude between the second EPSCs over the first EPSCs (i.e., EPSC2/EPSC1). To measure
217 AMPA/NMA ratio, NMDA-mediated current at +40 mV was measured at 50 ms after optogenetic
218 stimulation when AMPAR mediated-EPSCs decayed to the baseline. Series resistance (R_s) was
219 continuously monitored during recordings and only cells showed stable R_s < 20 MΩ with less
220 than 15% changes were proceeded for further analysis. Details of this procedure can be found
221 here: https://www.protocols.io/view/brain-slice-preparation-for-electrophysiology-reco-
222 36wgqj2eovk5/v1
223
224 **Perfusion and immunohistochemistry staining**
225 Mice were intraperitoneally injected with avertin for anesthesia followed by transcardial
226 perfusion using 1x PBS and 4% paraformaldehyde (PFA, pH = 7.4). After perfusion, the brains
227 were extracted and kept in 4% PFA overnight for post-fixation, and then were re-sectioned at a
228 70 µm thickness using a vibratome (VT1000s, Leica Biosystems, Buffalo Grove, IL).
229 https://www.protocols.io/view/standard-operating-procedure-mouse-transcardiac-pe-
230 3byl4b8r8vo5/v1
231

232 Brain sections were rinsed with 1x PBS for 3 times before performing
233 immunohistochemistry, followed by incubation with 1x PBS containing 0.5% Triton X-100 (PBS-T)
234 plus 2% normal donkey serum (Millipore Sigma) at room temperature for 60 min. They were
235 then incubated in the PBS-T with primary antibodies overnight at room temperature or 48 hours
236 at 4°C. The primary antibodies utilized in this study were: rabbit anti-pS129 α-Syn (1:10,000,
237 Bioscience Cat# 1536-1, RRID: AB_562180), mouse anti-NeuN (1:500, Millipore Cat# MAB377,
238 RRID: AB_2298772), mouse anti-vGluT1 (1:1,000, Synaptic Systems Cat# 135 011,
239 RRID:AB_2617087), guinea pig anti-vGluT2 (1:1,000, Synaptic System Cat# 135404, RRID:
240 AB_887884). The sections were then thoroughly rinsed with 1x PBS for 3 times before
241 incubating with the secondary antibodies (1: 500, AlexaFluor 594 donkey anti-rabbit IgG, Cat#
242 711-585-152, Jackson ImmunoResearch Labs, RRID: AB_2340621; AlexFluor 594 donkey anti-
243 mouse IgG, Cat# 715-586-150, Jackson ImmunoResearch Labs, RRID: AB_2340857; AlexaFluor
244 488 donkey anti-guinea pig IgG, Cat# 706-545-148, Jackson ImmunoResearch Labs, RRID:
245 AB_2340472) at room temperature for 2 hours. To reveal morphology of biocytin-labeled
246 neurons, brain slices were incubated with Cy5-conjugated streptavidin (SA1011, Thermo Fisher
247 Scientific) at a concentration of 1: 500 at room temperature for 2 h. Brain slices were then
248 rinsed using 1x PBS for 3 times before mounting on glass slides with the Vectorshield antifade
249 mounting medium (H-1000, Vector Laboratories). Slides were left at room temperature
250 overnight before sealing with nail oil and imaging. Details of immunofluorescent staining can be
251 found here: https://www.protocols.io/view/immunofluorescent-staining-3byl4bq9ovo5/v1
252
253 **Confocal imaging and analysis**

254 Confocal images were taken using a Nikon A1R microscope. Images of α-Syn pathology in BLA
255 were collected by a 20x objective lens and then analyzed using imageJ (RRID: SCR_003070, NIH,
256 https://imagej.net). To quantify the cortical and thalamic axon terminals in the BLA, vGluT1 and
257 vGluT2 immunoreactivity were imaged using a Nikon A1R confocal microscope under an oil
258 immersion 100x objective lens (NA=1.45; x/y, 1024 x 1024 pixels; z-step = 150 nm). All confocal
259 images were acquired using the identical microscope and camera settings. VGluT1 and vGluT2
260 density were stereologically quantified using optical dissector methods (dissector height = 3 µm
261 with a guard zone of 0.15 µm; counting frame = 10 x 10 µm) [38]. Images of NeuN staining were
262 taken from the BLA by a 60x objective (NA=1.40; x/y, 1024 x 1024 pixels; z-step = 1 µm) and
263 subjected to quantification using Imaris software (RRID: SCR_007370, version 10.0, Oxford, UK,
264 https://imaris.oxinst.com). ChR2-eYFP expression in mPFC was imaged using a Nikon Ni-U
265 fluorescence microscope under 2x objective lens. For morphology analysis, biocytin-filled
266 neurons were imaged using the confocal microscope under 20x objective lens (NA=0.75; x/y,
267 1024 x 1024 pixels; z-step = 1 µm). Morphology of biocytin-labelled neurons of BLA was
268 reconstructed followed by Sholl analysis using the Imaris software (RRID: SCR_007370, version
269 10.0, Oxford, UK, https://imaris.oxinst.com). Spines of the biocytin-filled neurons were imaged
270 by the confocal microscope under 100x objective lens (NA=1.45; x/y, 1024 x 1024 pixels; z-step =
271 500 nm). To quantify the spine density of BLA neurons, dendritic segments of 20 µm in length
272 were reconstructed and number of spines were counted. Images from controls and PFFs
273 injected mice were collected under identical settings in the confocal microscope and analyzed
274 by a researcher blinded to treatments. Details of digital imaging analysis can be found here:
275 https://www.protocols.io/view/confocal-imaging-and-digital-image-analysis-3byl4jmxzlo5/v1.

276

277 **Animal behaviors**

278 To assess motor function, animals were subject to locomotion and rotarods tests. For open field
279 locomotion test, the animal was placed in the empty open field (40 x 40 x 30 cm, W x L x H) and
280 allowed to explore for 10 min. Animal's locomotor activity was continuously recorded and
281 analyzed using ANYmaze software (Stoelting Co., Wood Dale, IL). For rotarod test, the animal
282 was placed on an accelerating rod (speed of 4-40 rpm in 5 min, San Diego Instruments, CA) and
283 the latency of fall was monitored and recorded. Detailed protocol of motor activity assays can
284 be found here: https://www.protocols.io/view/open-field-locomotion-test-e6nvwjxmdlmk/v1.
285 To assess animals' social interaction behavior, mice were placed to three-chamber apparatus
286 (MazeEngineers, Skokie, IL) with left, middle, and right chambers (20 x 13.5 cm^2). A round wire
287 cage (10 cm in diameter, 20 cm in height) was placed in the left and right chambers for novel
288 stimulus mouse. The stimulus mice were habituated to the wire cages for 20 min before the
289 testing day. The testing mice were habituated to the behavior room for at least 30 min before
290 the experiment. Three sessions were conducted during the testing day, including the
291 habituation, the session 1, and the session 2. The testing mice were habituated to the middle
292 chamber for 5 min before opening the doors to allow the mice freely explore the three
293 chambers for 10 min. During the first session, the testing mice were allowed to explore the
294 three chambers for a total of 10 min with one empty cage and the presence of a stimulus
295 mouse in the other wire cage. In the second session, the same testing mouse was allowed to
296 explore the three chambers for another 10 min with the presence of the familiar mouse in one
297 cage and a second never-met stimulus mouse in another wire cage. Mice movements were

298 tracking and the time spent in each chamber was quantified by AnyMaze software (Stoelting
299 Co.). Between each testing, the chamber was thoroughly cleaned with 70% ethanol to eliminate
300 the odor of mice.
301
302 **Data analysis and statistics**
303 Electrophysiology data were analyzed using Clampfit 11.1 (RRID: SCR_011323, Molecular
304 Devices, San Jose, USA). The amplitude of monosynaptic glutamatergic EPSCs were quantified
305 from an average of three sweeps. Confocal images were analyzed using Image J (RRID:
306 SCR_003070, NIH, https://imagej.net) and Imaris (RRID: SCR_007370, Oxford, UK,
307 http://www.bitplane. com/imaris). Statistics were performed in Prism 10 (RRID: SCR_002798,
308 GraphPad Software, http://www.graphpad.com). Non-parametric, distribution-independent
309 Mann-Whiney U (MWU) test was used for statistical comparison of data from two groups. The
310 amplitude of Cortico-BLA EPSCs across a range of stimulation and Sholl analysis were analyzed
311 using two-way analysis of variance (ANOVA) with *post hoc* Sidak's analysis multiple comparison's
312 test. All tests were two-tailed, and p-value < 0.05 was considered as statistical significance.

Results

Time-course of α-Syn pathology development in the BLA

We chose to employ the α-Syn preformed fibrils (PFFs)-based mouse models to interrogate circuit events associated with α-Syn aggregation in the BLA microcircuits. In the PFFs-based models, fibrillar α-Syn species are reported to be internalized at the axon terminals, which then recruit endogenously expressed α-Syn to form insoluble inclusions. This process has been shown to start at the axons and propagate to somatic regions, followed by a potential spreading of pathologic species between cells [3, 20]. We injected α-Syn PFFs into the dorsal striatum of wildtype C57BL6 mice to induce the accumulation of α-Syn pathology in the brain, including broad cerebral cortical regions and the amygdala [3, 39, 40].

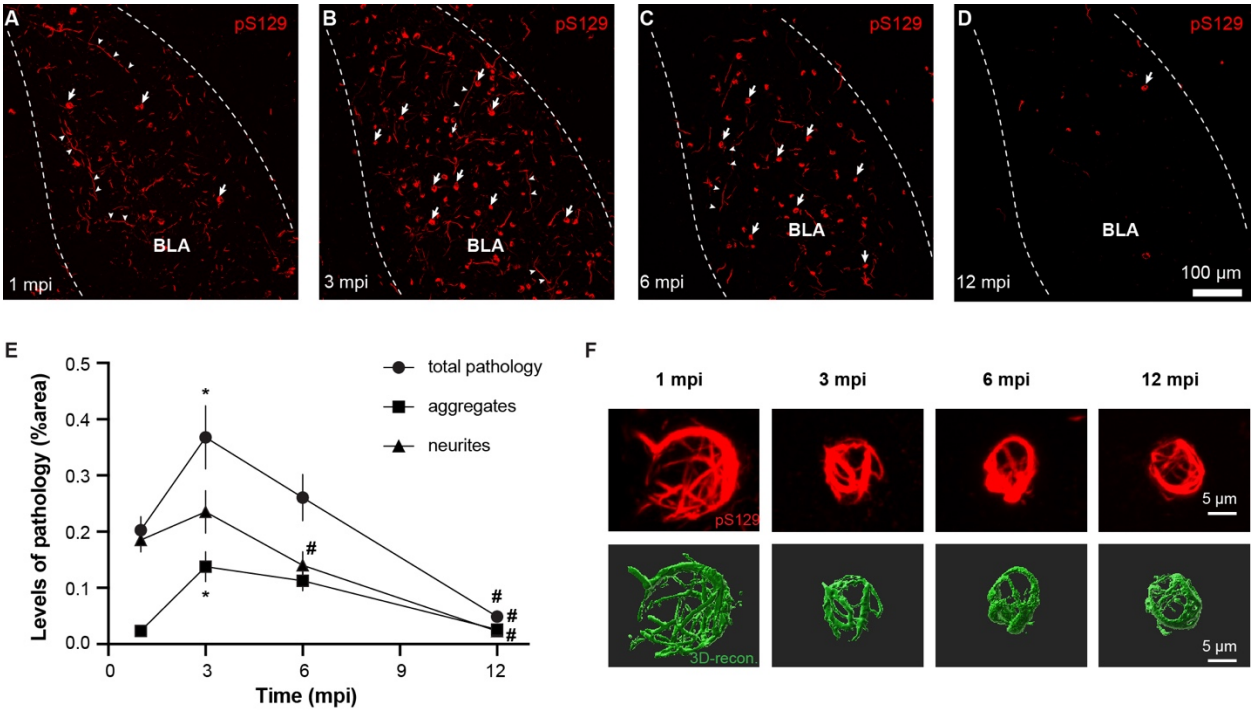

Figure 1. Time-course of αSyn pathology development in the BLA. A-D) Representative confocal images showing the development and accumulation of pS129⁺ pathology in the BLA at 1, 3, 6 and 12 months-post-injection (mpi). Arrows and arrowheads highlighted a few pS129⁺ somatic aggregates and neurites, respectively, in the BLA. **E)** Time course of the development of total α-syn pathology (filled circles), pS129⁺ somatic aggregates (square), and pS129⁺ neurites (triangle) in the BLA. Total α-Syn pathology, 1 mpi = 0.20±0.02, n = 38 slices/8 mice; 3 mpi = 0.37±0.06, n =

28 slices/10 mice; p = 0.004. pS129$^+$ aggregates, 1 mpi =0.02±0.005, n = 38 slices/8 mice; 3 mpi =0.14±0.03, n = 28 slices/10 mice, p < 0.0001. pS129$^+$ neurites, 1 mpi =0.19±0.02, n = 38 slices/8 mice, 3 mpi = 0.24±0.04, n = 28 slices/10 mice, p = 0.3. Total α-Syn pathology at 6 mpi = 0.26±0.04, n = 38 slices/10 mice, p = 0.09 versus total pathology at 3 mpi. pS129$^+$ aggregates at 6 mpi = 0.11±0.02, n = 38 slices/10 mice, p = 0.5 versus pS129$^+$ aggregates at 3 mpi. pS129$^+$ neurites at 6 mpi = 0.14±0.02, n = 38 slices/10 mice, p = 0.01 versus pS129$^+$ neurites at 3 mpi. Total α-Syn pathology at 12 mpi = 0.05±0.007, n = 35 slices/6 mice, p < 0.0001 versus total pathology at 3 mpi. pS129$^+$ aggregates at 12 mpi = 0.026±0.005, n = 35 slices/6 mice, p < 0.0001 versus pS129$^+$ aggregates at 3 mpi. pS129$^+$ neurites at 12 mpi = 0.02±0.0035, n = 35 slices/6 mice, p < 0.0001 versus pS129$^+$ neurites at 3 mpi.
*p< 0.05 relative to the counterparts at 1 mpi, #p < 0.05 relative to the counterparts at 3 mpi; one-way ANOVA. **F**) Representative images showing Lewy body-like somatic pS129$^+$ aggregates in the BLA at different time points (top panel) and their 3D reconstructions.

As expected, we detected robust phospho-Ser129 (pS129$^+$) α-Syn immunoreactivity in the BLA of PFFs-injected mice (**Figure 1A-D**), but not in the BLA of PBS-injected controls ("controls" hereinafter). α-Syn pathology in the BLA included both pS129$^+$ Lewy neurite (LN)-like and large Lewy body (LB)-like aggregates (**Figure 1A-D, F**), which are likely the α-Syn aggregation within the afferents and the somatic regions of glutamatergic principal neurons of the BLA, respectively [26, 39]. Next, we characterized the dynamic changes of α-Syn pathology abundance in the BLA at 1, 3, 6, and 12 months-post-injection (mpi). We measured the proportion of the BLA region covered by pS129$^+$ neurites, and pS129$^+$ somatic aggregates, as well as the total α-Syn pathology (i.e., pS129$^+$ LN/LB-like aggregates) to quantify α-Syn pathology load in the BLA, as in earlier studies (**Figure 1E**) [40, 41]. Specifically, moderate level of pS129$^+$ α-Syn pathology was detected in the BLA as early as at 1 mpi, which was dominated by the pS129$^+$ neurites (**Figure 1A, E**). The level of total pS129$^+$ α-Syn pathology continually grew beyond 1 mpi, peaking at 3 mpi (**Figure 1B, E**). After 3 mpi, the amount of total α-Syn pathology in the BLA remained at a relatively high at the 6 mpi timepoint but decreased significantly at 12 mpi (**Figure 1C, D, E**). Particularly, at 12 mpi only few pS129$^+$ somatic aggregates could be detected in the BLA, but nearly no LN-like structure could be seen in this region (**Figure 1D, E**).

357 Consistently, the reduced total α-Syn pathology in the BLA was initially driven by the loss of
358 pS129$^+$ neurites at 6 mpi (**Figure 1C, E**), and then by loss of both pS129$^+$ neurites and somatic
359 aggregates at 12 mpi (**Figure 1D, E**).
360 Furthermore, the LB-like somatic aggregates showed distinct morphological features
361 from early to later stages (**Figure 1F**). Specifically, the somatic aggregates became denser
362 gradually and smaller in size, which might be the process of maturation as reported by previous
363 studies [11, 42]. It is worth noting that maturation of Lewy bodies has been shown to drive
364 neurodegeneration in model systems, both *in vitro* and *in vivo* [11, 42]. These data suggest that
365 deposition of α-Syn pathology may compromise the integrity and function of BLA microcircuits
366 by disrupting synaptic connections followed by a possible loss of BLA neurons.
367
368 **α-Syn pathology induces neurodegeneration in the BLA at later stages**
369 Post-mortem studies of patients with advanced PD reported that the amygdala exhibits
370 significant Lewy body pathology and reduced cell density [32]. In experimental studies,
371 development and maturation of pS129$^+$ somatic aggregates have been reported to drive the
372 death of cortical glutamatergic neurons and SNc dopaminergic neurons in mice after more than
373 4 months post PFFs injections [3, 11, 42]. Thus, the gradual and robust reduction in the number
374 of pS129$^+$ somatic aggregates in the BLA from 6 to 12 mpi could have been the result of loss of
375 BLA neurons as the somatic aggregates mature (**Figure 1C-F**). To test this hypothesis, we
376 performed stereological quantification of BLA neurons at 6 and 12 mpi, prior to which
377 neurodegeneration is unlikely to occur in the BLA [3, 39]. The PFF-injected mice and controls
378 were perfusion-fixed using 4% PFA at 6 and 12 mpi and brain sections containing the BLA region

379 were collected and stained using anti-NeuN antibody as a pan-neuronal marker (**Figure 2**).

380 Relative to controls, the BLA of PFFs-injected mice showed a significant cell loss at 12 mpi

381 relative to controls, but not at 6 mpi (**Figure 2**), consistent with the findings of a recent study

382 using the same model [39]. These data suggest that deposition of α-Syn aggregates induced

383 neurodegeneration in the BLA at this late stage. The temporal relationship between the BLA cell

384 density reduction and the decrease in pS129^{+} somatic aggregates suggests that the decreased

385 LB-like aggregates can be attributed to degeneration of BLA neurons at 12 mpi as it has been

386 indicated in the literature [3, 40].

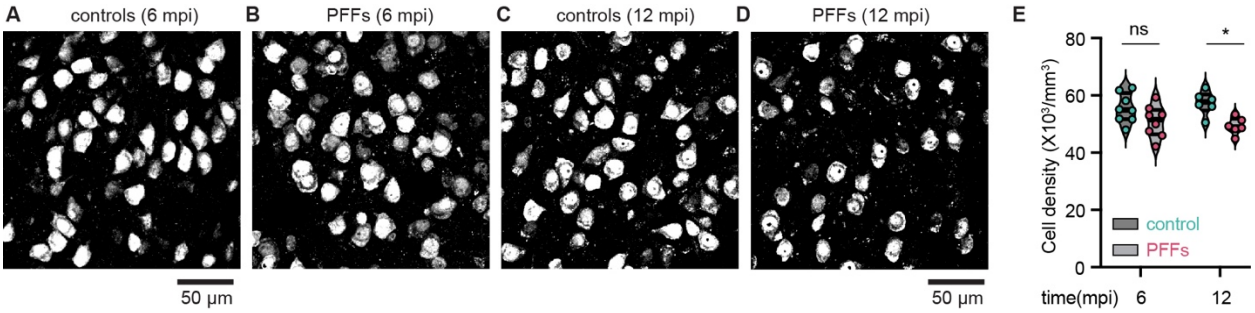

387

388 **Figure 2. α-Syn pathology induces neurodegeneration in the BLA at later stages. A-D**) Representative images
389 showing NeuN immunoreactivity in the BLA of controls (A, C) and PFFs-injected mice (B, D) at 6 mpi and 12 mpi. **E**)
390 Summarized results showing a reduced BLA cell density in the PFFs-injected mice relative to controls at 12 mpi, but
391 not at the 6 mpi. Cell densities at 6 mpi, control = 54.9 [51.7, 60.8] x10^3/mm^3, PFFs = 51.5 [46.4, 54.9] x10^3/mm^3, n =
392 8 mice/group, p = 0.16; Cell densities at 12 mpi, control = 57.7 [54.7, 60.3] x10^3/mm^3, PFFs = 48.9 [47.4, 51.8]
393 x10^3/mm^3, n = 6 mice/group, p = 0.0087, Mann-Whitney U (MWU) test.
394

395 **Loss of cortical afferents contributes to the decreased pS129^{+} neurites in the BLA**

396 Next, we tested the hypothesis that loss of glutamatergic inputs occurs prior to the BLA

397 neurodegeneration and further delineated the relative vulnerability of distinct glutamatergic

398 afferents to α-Syn pathology. The BLA receives major glutamatergic inputs from both the

399 cerebral cortices and the thalamus, the axons of which can be distinguished by the expression

400 of vesicular glutamate transporter (vGluT) 1 and 2, respectively. We recently reported that

401 vGluT1-expressing (vGluT1$^+$) cortical axons express higher levels of endogenous α-syn than
402 vGluT2$^+$ thalamic axons, rendering the cortical inputs more vulnerable to functional damages of
403 α-Syn aggregation than the thalamic inputs at 1 mpi [26]. Although at this early time point α-
404 Syn aggregation did not induce loss of cortico-BLA axon terminals, it remains to be determined
405 whether and when cortical axon degeneration occurs at later time points, as suggested by the
406 previous studies [20, 43].

407 Therefore, we extended our study to later time points and quantified the density of
408 vGluT1$^+$ puncta in the BLA as levels of α-Syn pathology evolves over time. Although the level of
409 pS129$^+$ α-Syn bearing neurites peaked at 3 mpi (**Figure 1E**), there was no change in the density
410 of vGluT1$^+$ puncta in the BLA at this stage (**Figure 3A**), indicating no loss of cortico-BLA axon
411 terminals at 3 mpi. However, a significant reduction in the density of vGluT1$^+$ puncta in the BLA
412 was detected at 6 and 12 mpi (**Figure 3B-C**), indicating a gradual loss of cortico-BLA axonal
413 projections. It is worthy to note that the time course of vGluT1$^+$ puncta reduction aligns with the
414 changes in pS129$^+$ neurites in the BLA (**Figure 1E**), suggesting that loss of cortico-BLA axonal
415 projections could contribute to the reduced pS129$^+$ neurites in the BLA at 6 and 12 mpi, though
416 a downregulation of vGluT1 protein itself cannot be excluded.

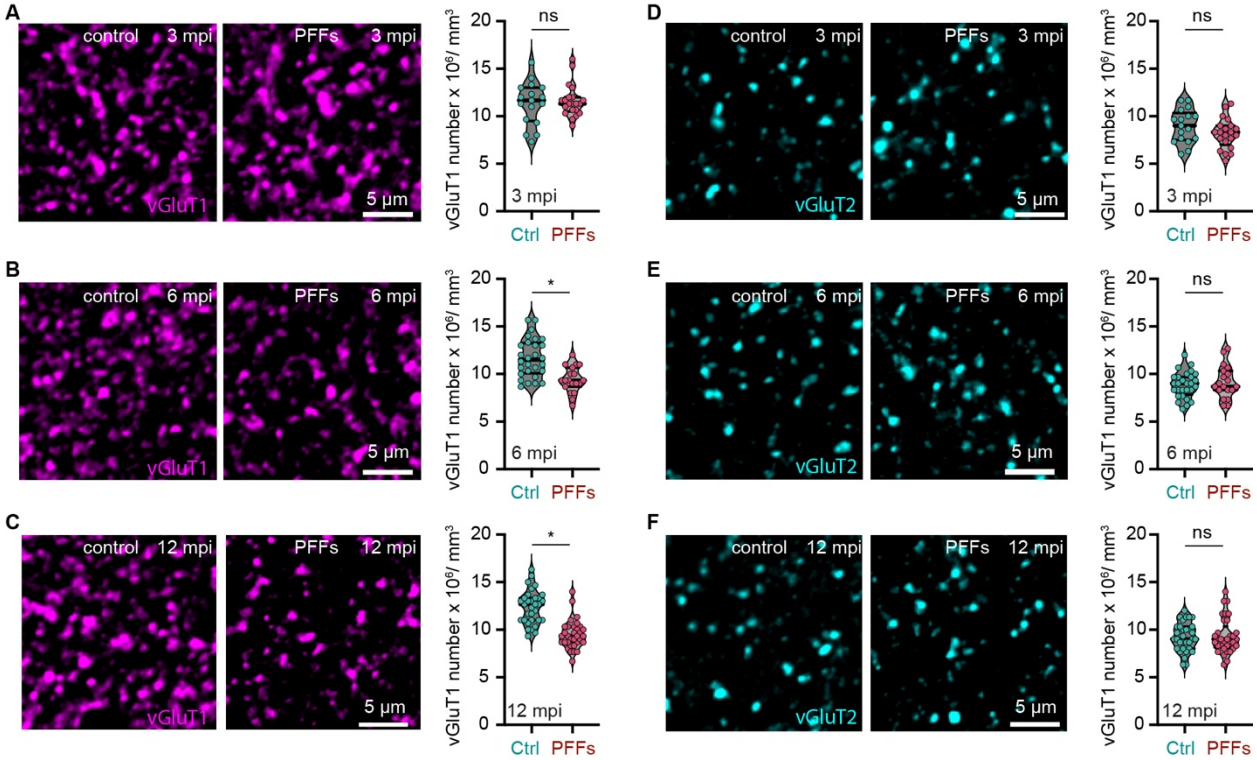

Figure 3. Loss of cortical afferents contributes to the decreased pS129⁺ neurites in the BLA. A-C) *Left*, representative confocal images showing vGluT1 immunoreactive puncta in the BLA of controls and PFFs-injected mice at 3, 6, and 12 mpi. *Right*) Summarized result showed changes in vGluT1 densities in the BLA at 3, 6, and 12 mpi. *A,* vGluT1 densities at 3 mpi, controls = 11.7 [9.5, 13], PFFs = 11.3 [10.5, 12.0], p = 0.86. *B,* vGluT1 densities at 6 mpi, controls = 11.5 [10.1, 13.3], PFFs = 9.3 [8.7, 10.7], p = 0.0001. *C,* vGluT1 densities at 12 mpi, controls = 12. 7 [11.0, 13.3], PFFs = 9.3 [8.7, 10.3], p <0.0001. **D-F**) *Left*, representative confocal images showing vGluT2 immunoreactive puncta in the BLA of controls and PFFs-injected mice at 3, 6, and 12 mpi. *Right*) Summarized result showed no change in vGluT2 densities in the BLA at 3, 6, and 12 mpi. *D,* vGluT2 densities at 3 mpi, controls = 9.0 [7.5, 10.3], PFFs = 8.3 [7.0, 9.0], p = 0.1387. *E,* vGluT2 densities at 6 mpi, controls = 9.0 [7.8, 9.7], PFFs = 8.7 [8.3, 10.3], p = 0.4883. *F,* vGluT2 densities at 12 mpi, controls = 9.0 [8.0, 10.3], PFFs = 9.0 [8.2, 10.3], p = 0.8225. N = 21 slices/4 mice for 3 mpi, 19 slices/4 mice for 6 mpi, 33 slices/6 mice for 12 mpi. MWU test.

Even though vGluT2⁺ thalamic inputs are more resilient to α-Syn pathology, they could still be affected as secondary effects of α-Syn's detrimental impact on BLA microcircuits at late stages. Thus, we further tested whether PFFs-injected mice showed changes in thalamic input to the BLA relative to controls. To this end, we quantified vGluT2⁺ axon terminals and surprisingly found no change in the density of vGluT2⁺ puncta in the BLA of PFFs injected mice relative to respective controls at 3, 6, and 12 mpi (**Figure 3D-F**). These data indicate that thalamic-BLA axonal projections were not altered by the dynamic changes of α-Syn pathology

437 over time. We also concluded that thalamo-BLA afferents did not underlie the decreased pS129$^+$
438 neurites in the BLA between 6 mpi and 12 mpi (**Figure 1**).

439 The BLA neurons express abundant *SNCA* (α-Syn encoding gene) and develop robust LB-
440 like somatic aggregates in both human PD and animal models (**Figure 1**). Thus, it is plausible to
441 speculate that changes in dendritic morphology of BLA neurons may contribute to the reduced
442 pS129$^+$ neurites in the BLA at 6 and 12 mpi. We therefore employed *ex vivo* whole-cell patch-
443 clamp technique to fill retrobeads-labeled BLA principal neurons with biocytin followed by
444 confocal imaging of their dendrites (**Figure 4A-E**). By performing Sholl analysis, we found that
445 there was no change in the dendritic arborization and total length of biocytin-labeled BLA
446 neurons from PFFs-injected mice relative to those from controls at 3, 6, and 12 mpi (**Figure 4C-**
447 **H**). These results suggest that dendritic changes of BLA neurons were unlikely to contribute to
448 the reduction of pS129$^+$ neurites that we detected in the BLA (**Figure 1**).

449 Given the cortical and thalamic inputs mainly target dendritic spines, we further
450 quantified the density of dendritic spines of the biocytin labeled BLA neurons at 3, 6, and 12
451 mpi (**Figure 4I-N**). We found that BLA principal neurons exhibited a reduced density of dendritic
452 spines at 3 and 6 mpi (**Figure 4I, J, L, M**). Surprisingly, such reduction of dendritic spines was not
453 detected from BLA neurons at 12 mpi (**Figure 4K, N**), which might be due to the sampling bias at
454 this time point (see **Discussion**).

455 Taken together, although BLA neurons also developed robust α-Syn aggregates, changes
456 in their dendritic morphology may not contribute to the decreased pS129$^+$ neurites seen in the
457 BLA at 6 and 12 mpi. In addition, the above data suggest that in the BLA microcircuits, α-Syn
458 pathology triggers loss of presynaptic axon terminals and postsynaptic dendritic spines, which

may lead to a disconnection of the BLA from the cerebral cortex as α-Syn pathology accumulates in the brain.

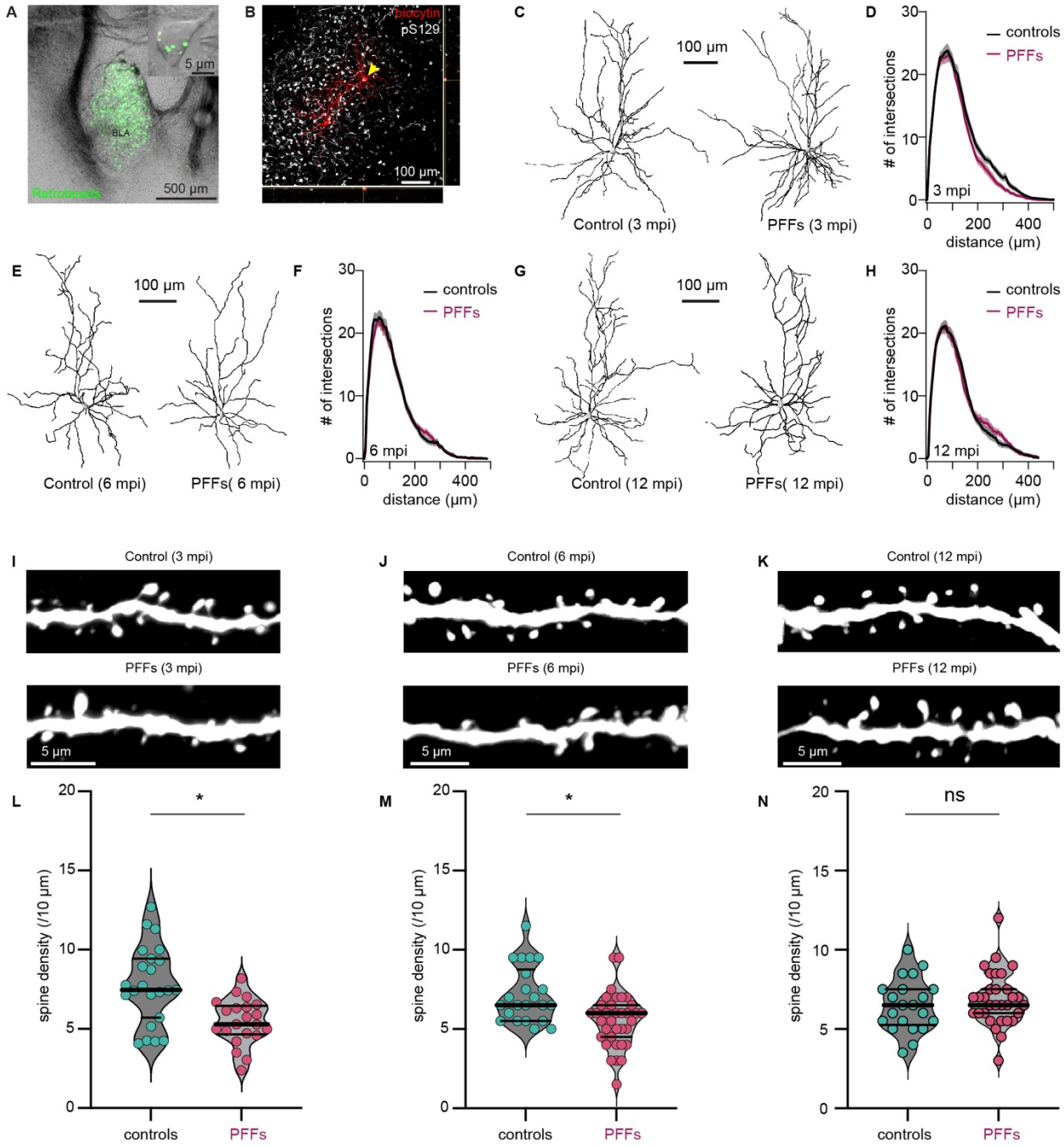

Figure 4. BLA principal neurons show moderate morphological changes as α-Syn pathology develops. A) Representative images showing green Retrobeads-labeled BLA neurons at low and high (inset) magnification. Cells with green beads labeling were targeted for biocytin filling and morphology analysis. **B**) Representative image

465 showing a Cy5-labeled BLA principal neurons against pS129$^+$ α-Syn immunoreactivity. This cell showed clear somatic
466 aggregation of pS129$^+$ α-Syn. **C**) *Left*, Representative 3D reconstructed BLA principal neurons from controls and PFFs-
467 injected mice at 3 mpi. *Right*, Summarized result from Sholl analysis showing the number of intersections at different
468 distance from the soma was similar between controls and PFFs-injected mice at 3 mpi. Thick and thin lines indicate
469 medians and interquartile ranges. **E-F**) Similar to C-D) expect at 6 mpi. **G-H**) Similar to C-D) expect at 12 mpi. **I-K**)
470 Confocal images showing representative dendritic spines of BLA neurons from controls and PFFs-injected mice at 3
471 (I), 6 (J), and 12 (K) mpi. **L-N**). Summarized results showing reduced dendritic spine densities of BLA neurons from
472 PFFs-injected mice relative to control at 3 (L) and 6 (M) mpi, but not at 12 (N) mpi. Spine densities at 3 mpi, controls
473 = 7.45 [5.7, 9.44]/10 μm; PFFs = 5.3 [4.66, 6.46]/10 μm, n= 21 segments/4 mice, p = 0.0008, MWU; Spine densities
474 at 6 mpi, controls = 6.5 [5.5, 8.75]/10 μm, PFFs = 6.0 [4.5, 6.5]/10 μm, n = 36 segments/4 mice, p =0.002, MWU;
475 Spine densities at 12 mpi, controls = 6.5 [5.25, 7.5]/10 μm, PFFs = 6.5 [6.0, 7.5]/10 μm, n = 31 segments/5 mice, p =
476 0.4, MWU test.
477

478 **α-Syn pathology disrupts functional connectivity between the mPFC and the BLA**

479 Next, we assessed the functional connectivity between the cerebral cortex and the BLA. Proper
480 interaction between the medial prefrontal cortex (mFPC) and the BLA plays a critical in
481 regulating emotion and social behavior [44-46]. Moreover, since both the mPFC and the BLA
482 accumulate robust α-Syn pathology following intrastriatal PFFs injection, the functional
483 connectivity between two regions could be impaired. Thus, we assessed how α-Syn pathology
484 affects mFPC-BLA connection at 3 and 6 mpi when the abundance of α-Syn pathology remains
485 high but has not yet caused severe degeneration of BLA neurons (**Figures 1E and 2**). We virally
486 expressed AAV9-hSyn-ChR2(H134R)-eYFP in the layer 5 projection neurons of the mPFC,
487 allowing a selective activation of mPFC-BLA inputs (**Figure 5A**). We optogenetically stimulated
488 ChR2(H134R)-expressing axon terminals in the BLA (**Figure 5A**) and recorded the evoked

489 excitatory postsynaptic currents (EPSCs) in the retrogradely labeled BLA principal neurons under
490 the voltage-clamp mode from controls and PFFs-injected mice (**Figure 5B, C**). The amplitude of
491 optogenetically-evoked, monosynaptic EPSCs were quantified to assess the connection strength
492 of mPFC-BLA synapses. A significant reduction of the amplitude of mPFC-BLA EPSCs was
493 detected in PFFs-injected mice relative to control at both 3 and 6 mpi (**Figure 5B, C**), indicating
494 an impaired functional connectivity of the mPFC-BLA synapses.

495 The reduced connection strength of mPFC-BLA synapses was accompanied by a
496 decreased ratio of amplitude of EPSCs mediated by AMPA receptors and NMDA receptors (i.e.,
497 AMPA/NMDAR ratio) in PFFs-injected mice relative to controls at both 3 and 6 mpi (**Figure 5D-**
498 **F**). Moreover, the ratio of EPSC2/EPSC1 at the mPFC-BLA synapses evoked by paired optogenetic
499 stimulation was also decreased in PFFs-injected mice relative to controls at both 3 and 6 mpi
500 (**Figure 5**), indicating an enhanced initial release probability of neurotransmitter at mPFC-BLA
501 input. Last, we did not detect changes in the connection strength of thalamo-BLA synapses in
502 PFFs-injected mice at 3 mpi (**Supplementary Figure 1**). Together with the changes in synaptic
503 markers (**Figure 3**), these data further suggest that cortico-BLA inputs were selectively
504 downregulated by α-Syn pathology whilst the thalamo-BLA synapses remained intact even at
505 later stages of α-Syn pathology.

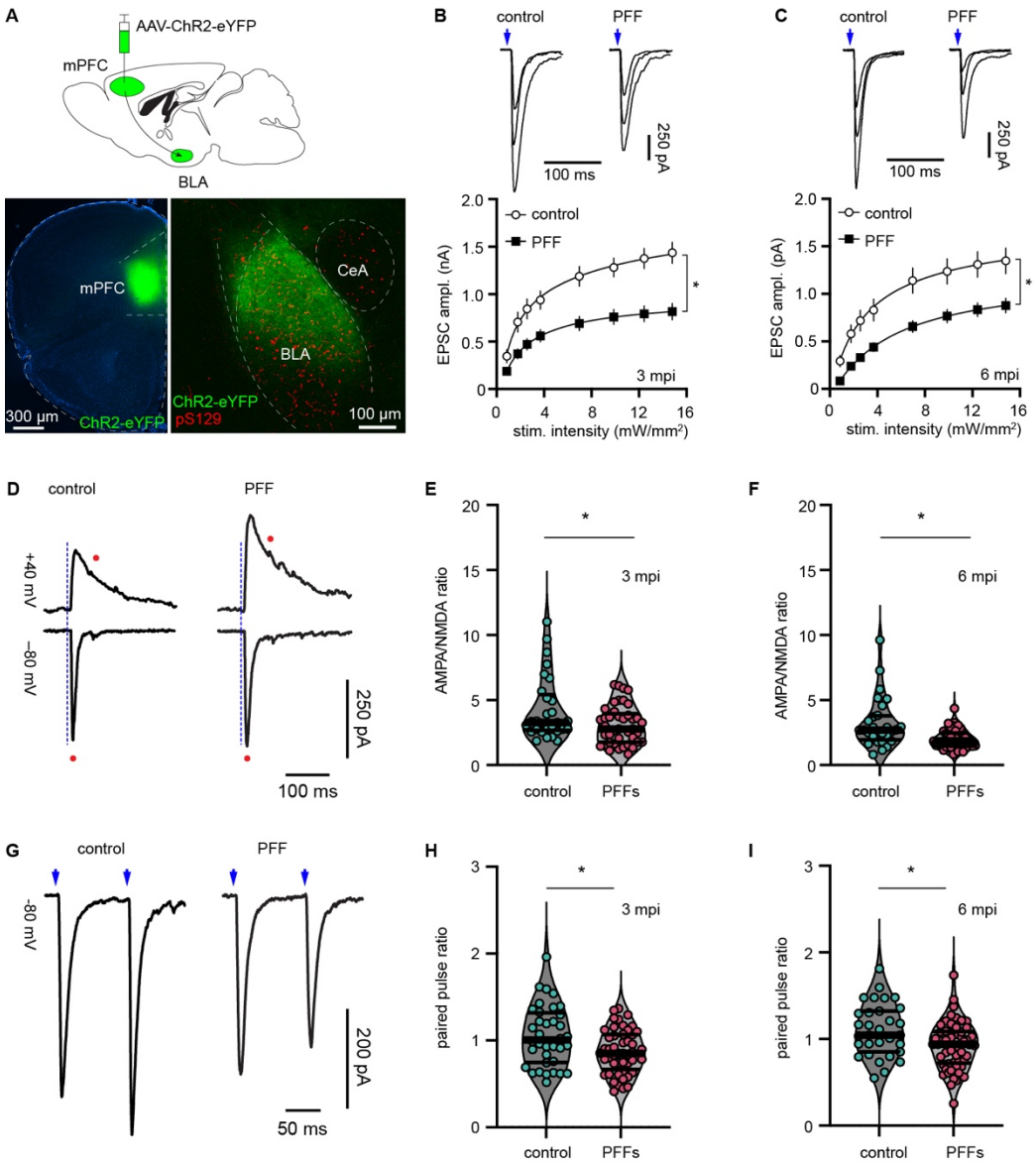

Figure 5. α-Syn pathology disrupts functional connectivity of the mPFC-BLA synapses. A) *Top*, diagram showing overall experimental design. *Bottom*, Representative AAV-ChR2-eYFP injection site in the mFPC (left) and the eYFP-labeled axonal terminal field in the BLA (right). **B-C**) Decreased amplitude of optogenetically evoked mPFC-BLA EPSCs in PFFs-injected mice relative to controls at both 3 (B) and 6 (C) mpi. *Top*) Representative traces of EPSCs evoked by optical stimulation intensities of 1.8, 3.6, and 12 mW/mm^2. Blue arrows indicate when the optogenetic stimulation was delivered. *Bottom*) Summarized graphs showing reduced amplitude of mPFC-BLA ESPCs across a range of stimulation intensities in PFFs-injected mice relative to controls at both 3 and 6 mpi. N = 44 cells/7 mice at 3 mpi and 57 cells/7 mice at 6 mpi. Two-way ANOVA followed by Sidak multiple comparisons test. **D**) Representative traces of mPFC-BLA EPSCs recorded at -80 mV and +40 mV from both controls and PFFs-injected mice. Red dots indicate where the AMPA receptor- and NMDA receptor-mediated EPSCs were measured at -80 mV and +40 mV, respectively. Blue dashed lines indicate when optogenetic stimulation was delivered. **E-F**) Summarized result showing reduced AMPA/NMDA ratios at mPFC-BLA synapses in PFFs-injected mice relative to controls at 3 mpi (E, control = 3.3 [2.7, 5.4], n = 29 cells/4 mice, PFFs = 2.8 [1.8, 4.0], n = 41 cells/7 mice, p = 0.05) and 6 mpi (F, control = 2.7 [1.9, 3.8], n = 28 cells/4 mice, PFFs = 1.9 [1.5, 2.5], n = 46 cells/6 mice, p = 0.0006) . **G**) Representative traces of mPFC-BLA EPSCs evoked by paired optogenetic stimulation pulses at -80 mV in both controls and PFFs-injected mice. Blue arrows indicate when the optogenetic stimulation was delivered. **H-I**) Summarized results showing reduced ratios of

523 EPSC2/EPSC1 at the mPFC-BLA synapses in PFFs-injected mice relative to controls at both 3 mpi (H, control = 1 [0.75,
524 1.32], n = 36 cells/5 mice; PFFs = 0.85 [0.67, 1.1], n = 48 cells/7 mice, p = 0.016, MWU) and 6 mpi (I, control = 1.04
525 [0.85, 1.32], n = 31 cells/4 mice, PFFs = 0.94 [0.72, 1.09], n= 57 cells/7 mice, p = 0.008, MWU test).
526

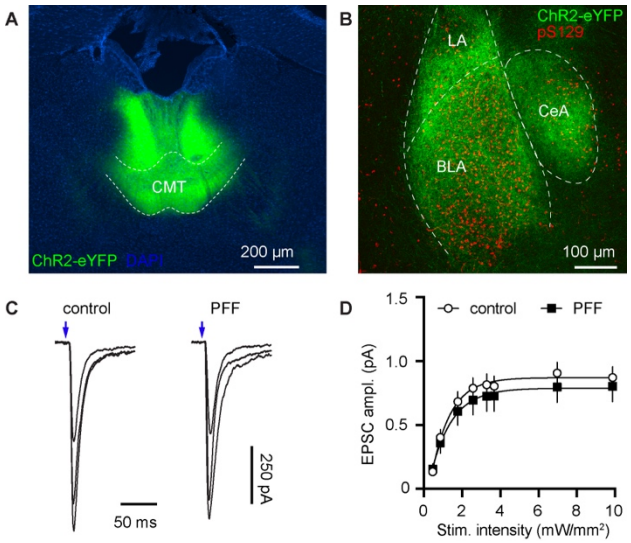

527

528 **Supplementary Figure 1. Thalamic inputs to the BLA were not affected by the α-Syn pathology. A)** Representative
529 AAV-ChR2-eYFP injection site in the thalamic region. **B**) Representative image showing eYFP-labeled thalamic axon
530 terminal field in the amygdala. **C-D**) Representative optogenetically-evoked thalamo-BLA EPSCs in controls and PFFs-
531 injected mice at 3 mpi (C) and the summarized results (D), Two-way ANOVA followed by Sidak multiple comparisons
532 test.

533

534 **Social interaction behavior is impaired by α-Syn pathology and rescued by chemogenetic**
535 **activation of mPFC-BLA pathway**

536 Given the robust disconnection between the mPFC and the BLA (**Figure 5**), we next attempted
537 to determine whether the impaired mPFC-BLA projection affects amygdala-dependent behavior.
538 We performed behavioral tests using both controls and PFFs-injected mice at 3 mpi when the α-
539 Syn pathology remained at peak level but has not yet resulted in robust presynaptic structural

540 changes at the cortico-BLA synapses and loss of BLA neurons (**Figures 2 and 3**) making
541 functional rescue still possible.
542 Considering the functional impairment of the mPFC-BLA connections at 3 mpi, we
543 further tested the hypothesis that development of α-Syn pathology leads to impaired social
544 interaction behavior. We chose the 3-chamber sociability test, as the performance in this test is
545 dependent on an intact amygdala microcircuit as well the interaction between the BLA and the
546 mPFC [44, 47, 48]. Each test began with 10 min habituation to the behavior apparatus with two
547 empty cages. During the habituation, both controls and PFF-injected mice spent comparable
548 amount of time in the left and right chambers of the empty cage. This result indicates that
549 neither controls nor PFFs-injected mice exhibited baseline preference of either chamber. Next, a
550 stimulus mouse was placed into one empty cage (S1, **Figure 6A**), and the test mouse was then
551 allowed to explore both chambers (session I in **Figure 6A**). Both controls and PFF-injected mice
552 spent significantly more time with the never-before-met stimulus mouse S1 than that with the
553 non-social empty cage (**Figure 6A, B, D**). This result suggests that PFFs-injected mice exhibit
554 normal sociability relative to controls. Next, we studied social novelty preference of PFFs-
555 injected mice. To do this, we added a second novel stimulus mouse 2 (S2) into the empty cage in
556 the presence of the familiar stimulus S1 to evaluate the test mouse's interest in the familiar
557 social stimulus *versus* the novel one when both were present (see the session 2 in **Figure 6A, C**).
558 While controls spent much more time with the novel stimulus (S2) relative to the familiar one
559 (S1), PFFs-injected mice spent similar amount of time with either the familiar stimulus (S1) or
560 the novel stimulus (S2) (**Figure 6C, E**).

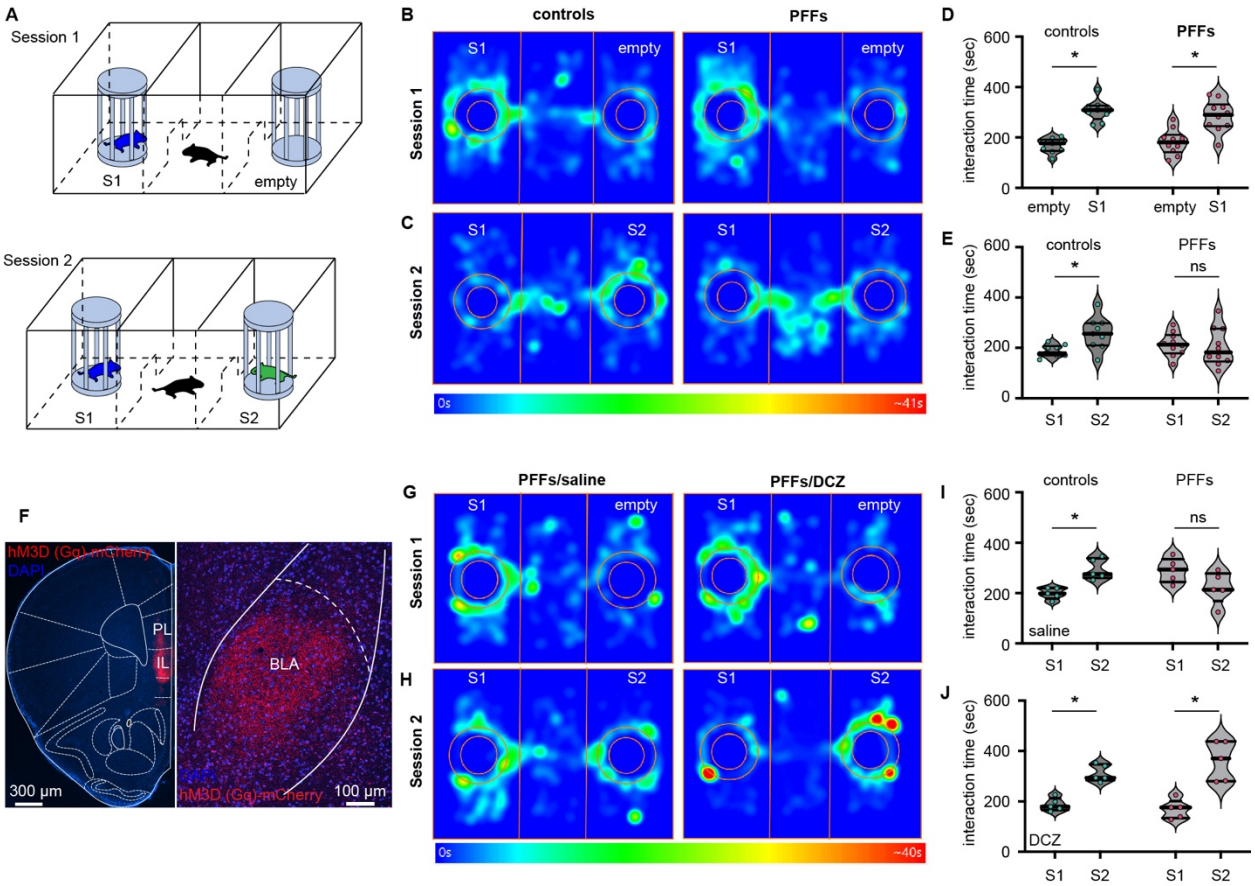

Figure 6. Social interaction behavior was impaired by α-Syn pathology and rescued by chemogenetic activation of mPFC-BLA pathway. A) Diagram showing overall behavioral experimental design. **B**) Representative heatmap plots showing social interaction behavior of controls and PFFs-injected mice in the Session 1 when S1 was paired with an empty cage for sociability. **C**) Representative heatmap plots showing social interaction behavior of controls and PFFs-injected mice in the Session 2 when familiar S1 was paired with a novel stimulus S2 for social novelty preference. **D-E**) Summarized graphs showing a normal sociability (D, controls empty = 177 [147, 191] sec, control S1 = 309 [273, 326] sec, n = 9 mice, $p < 0.0001$; PFFs empty = 181 [142, 211] sec, PFFs S1 = 290 [245, 331] sec, n = 10 mice, $p = 0.001$, MWU) but impaired social novelty preference behavior of PFFs-injected mice relative to controls (E, control S1 = 179 [170, 207] sec, control S2 = 256 [210, 298] sec, n= 9 mice, $p = 0.01$, MWU; PFFs S1 = 213 [179, 251] sec, PFFs S2 = 182 [146, 276] sec, n = 10 mice, $p = 0.49$, MWU). **F**) Representative image showing AAV-fDIO-hM3D(Gq)-mCherry infection site in the mPFC and the mCherry-labeled mFPC axon terminal field in the BLA. **G**) Representative heatmap plots showing sociability of PFFs-injected mice receiving either saline or DCZ (DREADDs agonist) administration. **H**)

Representative heatmap plots showing social novelty preference of PFFs-injected mice receiving either saline or DCZ (DREADDs agonist) administration. **I-J**) Summarized graphs showing that PFFs-injected mice receiving saline injections exhibit impairment in their social novelty preference behavior of (I, saline-injected control, S1 = 198 [178, 220] sec, S2 = 275 [260, 338] sec, n = 5 mice, p = 0.008; saline-injected PFFs, S1 = 294 [244, 335] sec, S2 = 214 [168, 278] sec, n =5 mice, p = 0.09, MWU), which was rescued by DREADDs agonist DCZ injection (J, DCZ-injected controls, S1 = 180 [166, 213] sec, S2 = 294 [284, 347] sec, n = 5 mice, p = 0.008; DCZ-injected PFFs, S1 = 176 [134, 201] sec, S2 = 371 [280, 438] sec, n = 5 mice, p = 0.008, MWU).

It is important to note that relative to controls, PFFs-injected mice at 3 mpi showed comparable general motor activity in locomotion test and rotarod test and similar levels of anxiety elevated plus maze as measured by the time spent in open arms (**Supplementary Figure 2**). These data were consistent with previous report [3, 39, 40] and suggested that PFFs-injected mice do not develop parkinsonian motor deficits or enhanced anxiety, which is important as such behaviors could confound the social interaction behavioral test. Taken together, these results suggested that PFFs-injected mice exhibited impaired social novelty preference and were not able to distinguish between familiar- and novel-stimuli.

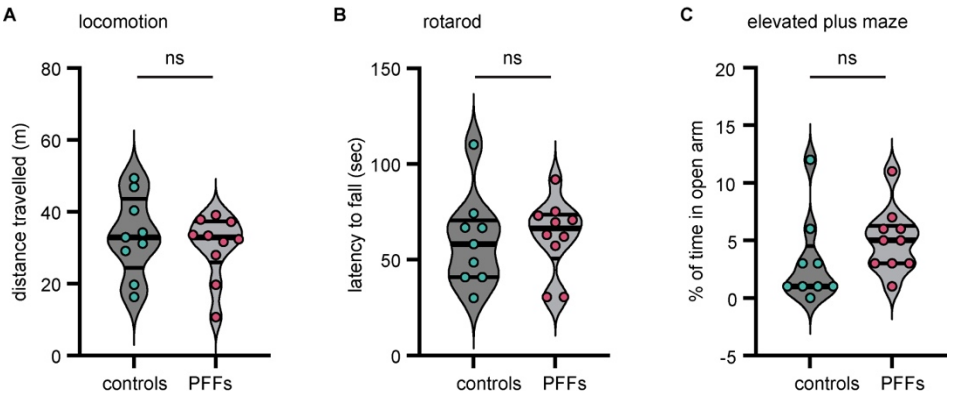

592 **Supplementary Figure 2. PFFs-injected mice showed normal motor function and anxiety level at 3 mpi. A-C**)
593 Summarized graphs showing no difference between controls and PFFs-injected mice in the locomotion test (A,
594 distance travelled, control = 33 [24, 44] m, n = 9 mice, PFFs = 33 [26, 37], n = 10 mice, p = 0.7, MWU), the rotarod
595 test (B, latency to fall, control = 58 [41, 71] sec, n = 9 mice, PFFs = 66 [51, 74] sec, n = 10 mice, p = 0.5, MWU) and
596 the elevated plus maze (C, % of time in open arm, control = 1 [1, 4.5]%, n= 9 mice, PFFs = 5 [3, 6]%, n = 10 mice, p =
597 0.08, MWU).
598
599 Interestingly, while the mPFC-BLA projections showed significant functional impairment
600 in PFFs-injected mice at 3 mpi, their presynaptic axonal terminals remained largely intact
601 (**Figures 3 and 5**). Given the critical role of mPFC inputs to the BLA in regulating social
602 interaction, we sought to determine whether the deficient social novelty preference behavior
603 could be rescued via activation of mPFC-BLA connections in PFFs-injected mice. To this end, we
604 injected retrograde AAV-FlpO into the BLA and AAV-fDIO-hM3D(Gq)-mCherry into the mFPC
605 (**Figure 6F**). This intersectional approach allows us to selectively stimulate mPFC-BLA synaptic
606 neurotransmission using a chemogenetic approach. Three weeks after viral infections, PFFs-
607 injected mice were subject to intraperitoneal injections of saline or deschlorozapine (DCZ)
608 followed by social novelty preference behavior test. After saline injection, while controls
609 showed normal social novelty preference, PFFs-injected mice were not able to distinguish novel-
610 *versus* familiar-stimulus mice (i.e., S2 *vs* S1, **Figure 6F**), consistent with our data from previous
611 cohort of animals (**Figure 6A-D**). In contrast, when PFFs-injected mice were subject to social
612 novelty preference test after DCZ injection, they showed strong preference to S2 *versus* S1
613 (**Figure 6I**), suggesting that their impaired social novelty preference has been rescued by

614 chemogenetic stimulation of mPFC-BLA connection (**Figure 6H, J**). Control mice showed normal

615 social novelty preference following DCZ injection (**Figure 6J**).

616 Altogether, the above data suggest that the social novelty preference was disrupted by

617 α-Syn pathology in PFFs-injected mice at 3 mpi. Importantly, such disruption correlated with

618 impaired mPFC-BLA synaptic connection, which was then rescued by chemogenetic stimulation

619 of the mPFC-BLA connection in the PFFs-injected mice.

620

621 **Discussion**

622 The present work studies circuitry events associated with the development of α-Syn pathology
623 in mouse brain. By performing detailed anatomical and physiological analyses at multiple time
624 points after triggering α-Syn pathology, we provided novel insight into how α-Syn aggregation
625 impairs the connectivity and function of complex amygdala microcircuits. While most research
626 in the field has focused on the processes that initiate, facilitate, and/or exacerbate α-Syn
627 pathology formation and propagation, the present work highlights the less explored, yet
628 important, circuitry dysfunction associated with α-Syn aggregation that can underlie some of
629 the symptoms manifested by individuals afflicted by synucleinopathies. These studies are of
630 clinical relevance as strategies to prevent worsening of α-Syn pathology and to repair the
631 damaged circuits could make the current treatments for diseases like PD and DLB more
632 effective.

633

634 **Synaptic dysfunction occurs earlier than neurodegeneration in the BLA**

635 We demonstrated that α-Syn aggregation compromises synaptic function before structural
636 changes occur, including the loss of presynaptic axon terminal markers. In the context of our
637 recent work, even though functional deficits of cortico-BLA synapse may occur as early as 1 mpi
638 [26], but loss of cortico-BLA presynaptic marker vGluT1 was only detected at the 6 mpi
639 timepoint (**Figure 3**). Moreover, BLA neurons are also prone to accumulating α-Syn aggregates,
640 which perhaps results in the loss of spines at 3 mpi (**Figure 4**) and their degeneration at much
641 later stages, i.e., 12 mpi (**Figure 2**). These observations are consistent with reports from the

642 nigrostriatal system in parkinsonian animals, showing deficits in dopamine release and
643 degeneration of axons prior to severe degeneration of dopaminergic neurons [4, 6, 21, 49, 50].
644 It is important to note that while BLA neurons exhibited loss of dendritic spines, the
645 initial release probability at cortico-BLA synapses increased at 3 and 6 mpi (**Figure 5**). This
646 observation is consistent with earlier findings from cultured hippocampal neurons, in which the
647 loss of postsynaptic spines and a paradoxical increase of presynaptic glutamate release were
648 reported [51]. Froula *et al* suggested that the enhanced presynaptic release probability might be
649 due to an increased size of readily releasable pool of neurotransmitters. Surprisingly, our
650 analysis showed that the dendritic spine density of BLA neurons returned to control levels at 12
651 mpi (**Figure 4**). It is however worth mentioning that this unexpected observation (as well as no
652 change in dendritic length of BLA neurons, Figure. 4G) can be the result of sampling bias during
653 our cell selection process for biocytin labeling at 12 mpi, because targeting dying and shrunk
654 cells is technically challenging. Overall, this can lead to an overrepresentation of healthier BLA
655 neurons in our dataset that are resilient to α-Syn pathology.
656
657 **Synaptic dysfunction is sufficient to drive the manifestation of behavioral phenotypes**
658 At the early stage of α-Syn based models, functional alterations of nigrostriatal pathway have
659 been reported to underlie the manifestation of parkinsonian motor deficits [4, 21, 52, 53]. In
660 the present study, we found that, prior to the loss of BLA neurons, mPFC-BLA synapses exhibited
661 functional impairment in PFFs-injected mice at 3 mpi, which temporally correlated with the
662 manifestation of defected social interaction behavior (**Figures 5 and 6**). Interestingly, the
663 impaired social novelty preference behavior was rescued by chemogenetic stimulation of the

664 defected mPFC-BLA pathway. Together, these findings support the hypothesis that synaptic
665 dysfunction is sufficient to drive the manifestation of behavioral phenotypes. The intrastriatal
666 PFFs-injected mice exhibited very specific deficits in emotion related behavior. For example,
667 while they exhibited deficits in social novelty preference (**Figure 6**) and social dominance
668 behavior [39], no change in their anxiety levels in the elevated plus maze test were detected
669 (**Supplementary Figure 2**, also see [39, 40]). Though compelling evidence suggests that both
670 social behavior and anxiety are tightly regulated by the amygdala, it is plausible that
671 performance in the elevated plus maze test may involves distinct amygdala subcircuits from
672 those activated during the 3-chamber social interaction test [54, 55].
673
674 **Cell type-specific α-Syn expression and its implications in circuit dysfunction**
675 In a complex circuit, not all afferents within the same neurochemical category are
676 equally affected by α-Syn aggregation. For example, vGluT2^{+} glutamatergic axons arising from
677 the thalamus are more resilient relative to vGluT1^{+} axons in the BLA, even at a later stage (e.g.,
678 12 mpi, **Figure 4**). This observation is largely consistent with lower *Snca* mRNA levels in thalamic
679 neurons as well as α-Syn expression in their axon terminals [26, 56]. Moreover, evidence in the
680 literature consistently reports that Lewy body-like pS129^{+} somatic aggregates are more
681 abundant in cerebral cortical regions relative to thalamic regions in intrastriatal PFFs models [3,
682 26, 40, 41, 57], suggesting that the cerebral cortex and thalamus are affected differently by α-
683 Syn pathology in diseased state. Of relevance to the present work, it is known that cooperative
684 activity and plasticity of cortical and thalamic inputs are essential to normal amygdala function
685 in the formation and long-term storage of emotion memory [58, 59]. It remains to be

686 determined how the disrupted balance or cooperation of cortical and thalamic inputs to the BLA
687 might impair emotion encoding and regulation by the amygdala circuits. Remarkably, human
688 imaging studies reported that PD individuals diagnosed with depression showed a reduced
689 activation of the amygdala in the presence of aversive stimulations as well as a disconnected
690 cortical (but not the thalamic) inputs to the amygdala [33, 36]. Our findings of weakened
691 cortical, but not thalamic inputs, to the BLA might be of relevance to this clinical observation in
692 PD individuals exhibiting neuropsychiatric symptoms.
693 The complicated interaction and impact of α-Syn pathology on circuit function can also
694 partially explain why emotion dysregulation, including anxiety and depression, can occur at any
695 stages of the disease in PD or DLB individuals (e.g., even before the onset of motor symptoms),
696 which might vary depending on where the α-Syn pathology starts and how it can affect specific
697 circuits. While the present studies focus on the impact of α-Syn pathology on the amygdala
698 function and related behavior, we must acknowledge that degeneration of key neuromodulators
699 and their inputs to the amygdala (e.g., dopaminergic and noradrenergic systems) also play key
700 roles in the development of neuropsychiatric symptoms in PD and DLB.
701
702 **Conclusion**
703 We presented a combination of anatomical and physiological evidence to demonstrate a series
704 of circuitry events occurred in the amygdala circuits associated with α-Syn pathology in mouse
705 brain. Our findings not only support several well-accepted concepts in the field (e.g., synaptic
706 deficits prior to neurodegeneration), but also highlight the fact that we need to consider circuit

707 complexity before we can gain a thorough understanding on the contribution of α-Syn to brain

708 function in health and in diseased states.

709

710

711 **List of abbreviations**

712 BLA basolateral amygdala

713 α-Syn α-synuclein

714 PD Parkinson's disease

715 DLB Dementia with Lewy bodies

716 SNc Substantia nigra pars compacta

717 PFFs α-Syn preformed fibrils (PFFs).

718 EPSCs excitatory postsynaptic currents

719 mPFC medial prefrontal cortex

720 DREADDs designer receptors exclusively activated by designer drugs

721 IL-mPFC infralimbic subregion of mPFC

722 aCSF artificial cerebrospinal fluid

723 R_s series resistance

724 PFA paraformaldehyde

725 ANOVA analysis of variance

726 $pS129^+$ phospho-Ser129

727 LN Lewy neurite

728 LB Lewy body

729 mpi months-post-injection

730 vGluT1 vesicular glutamate transporter 1

731 vGluT2 vesicular glutamate transporter 2

732 SNCA Alpha Synuclein

733 DCZ deschloroclozapine

734

735

References cited:

1. Spillantini MG, Schmidt ML, Lee VMY, Trojanowski JQ, Jakes R, Goedert M: **α-Synuclein in Lewy bodies.** *Nature* 1997, **388:**839-840.
2. McCann H, Stevens CH, Cartwright H, Halliday GM: **α-Synucleinopathy phenotypes.** *Parkinsonism & Related Disorders* 2014, **20:**S62-S67.
3. Luk KC, Kehm V, Carroll J, Zhang B, O'Brien P, Trojanowski JQ, Lee VMY: **Pathological α-Synuclein Transmission Initiates Parkinson-like Neurodegeneration in Nontransgenic Mice.** *Science* 2012, **338:**949-953.
4. Janezic S, Threlfell S, Dodson PD, Dowie MJ, Taylor TN, Potgieter D, Parkkinen L, Senior SL, Anwar S, Ryan B, et al: **Deficits in dopaminergic transmission precede neuron loss and dysfunction in a new Parkinson model.** *Proceedings of the National Academy of Sciences* 2013, **110:**E4016-E4025.
5. Kim S, Kwon S-H, Kam T-I, Panicker N, Karuppagounder SS, Lee S, Lee JH, Kim WR, Kook M, Foss CA, et al: **Transneuronal Propagation of Pathologic α-Synuclein from the Gut to the Brain Models Parkinson's Disease.** *Neuron* 2019, **103:**627-641.e627.
6. Ledonne A, Cenere MM, Paldino E, D'Angelo V, D'Addario SL, Casadei N, Nobili A, Berretta N, Fusco FR, Ventura R, et al: **Morpho-Functional Changes of Nigral Dopamine Neurons in an α-Synuclein Model of Parkinson's Disease.** *Movement Disorders* 2023, **38:**256-266.
7. Lundblad M, Decressac M, Mattsson B, Björklund A: **Impaired neurotransmission caused by overexpression of α-synuclein in nigral dopamine neurons.** *Proceedings of the National Academy of Sciences of the United States of America* 2012, **109:**3213-3219.
8. Li J-Y, Englund E, Holton JL, Soulet D, Hagell P, Lees AJ, Lashley T, Quinn NP, Rehncrona S, Björklund A, et al: **Lewy bodies in grafted neurons in subjects with Parkinson's disease suggest host-to-graft disease propagation.** *Nat Med* 2008, **14:**501-503.
9. Desplats P, Lee H-J, Bae E-J, Patrick C, Rockenstein E, Crews L, Spencer B, Masliah E, Lee S-J: **Inclusion formation and neuronal cell death through neuron-to-neuron transmission of α-synuclein.** *Proceedings of the National Academy of Sciences* 2009, **106:**13010-13015.
10. Praschberger R, Kuenen S, Schoovaerts N, Kaempf N, Singh J, Janssens J, Swerts J, Nachman E, Calatayud C, Aerts S, et al: **Neuronal identity defines α-synuclein and tau toxicity.** *Neuron* 2023, **111:**1577-1590.e1511.
11. Mahul-Mellier A-L, Burtscher J, Maharjan N, Weerens L, Croisier M, Kuttler F, Leleu M, Knott GW, Lashuel HA: **The process of Lewy body formation, rather than simply α-synuclein fibrillization, is one of the major drivers of neurodegeneration.** *Proceedings of the National Academy of Sciences of the United States of America* 2020, **117:**4971-4982.
12. Kim YE, Lai TT, Kim YJ, Jeon B: **Preferential microglial activation associated with pathological alpha synuclein transmission.** *J Clin Neurosci* 2020, **81:**469-476.
13. Peng C, Gathagan RJ, Covell DJ, Medellin C, Stieber A, Robinson JL, Zhang B, Pitkin RM, Olufemi MF, Luk KC, et al: **Cellular milieu imparts distinct pathological α-synuclein strains in α-synucleinopathies.** *Nature* 2018, **557:**558-563.

14. Johnson ME, Stecher B, Labrie V, Brundin L, Brundin P: **Triggers, Facilitators, and Aggravators: Redefining Parkinson's Disease Pathogenesis.** *Trends Neurosci* 2018, **42:**4-13.
15. Fares MB, Jagannath S, Lashuel HA: **Reverse engineering Lewy bodies: how far have we come and how far can we go?** *Nat Rev Neurosci* 2021, **22:**111-131.
16. Kordower JH, Olanow CW, Dodiya HB, Chu Y, Beach TG, Adler CH, Halliday GM, Bartus RT: **Disease duration and the integrity of the nigrostriatal system in Parkinson's disease.** *Brain* 2013, **136:**2419-2431.
17. Gonzalez-Rodriguez P, Zampese E, Stout KA, Guzman JN, Ilijic E, Yang B, Tkatch T, Stavarache MA, Wokosin DL, Gao L, et al: **Disruption of mitochondrial complex I induces progressive parkinsonism.** *Nature* 2021, **599:**650-656.
18. McGregor MM, Nelson AB: **Circuit Mechanisms of Parkinson's Disease.** *Neuron* 2019, **101:**1042-1056.
19. Galvan A, Wichmann T: **Pathophysiology of parkinsonism.** *Clinical neurophysiology* 2008, **119:**1459-1474.
20. Volpicelli-Daley Laura A, Luk Kelvin C, Patel Tapan P, Tanik Selcuk A, Riddle Dawn M, Stieber A, Meaney David F, Trojanowski John Q, Lee Virginia MY: **Exogenous α-Synuclein Fibrils Induce Lewy Body Pathology Leading to Synaptic Dysfunction and Neuron Death.** *Neuron* 2011, **72:**57-71.
21. Tozzi A, Sciaccaluga M, Loffredo V, Megaro A, Ledonne A, Cardinale A, Federici M, Bellingacci L, Paciotti S, Ferrari E, et al: **Dopamine-dependent early synaptic and motor dysfunctions induced by alpha-synuclein in the nigrostriatal circuit.** *Brain* 2021, **144:**3477-3491.
22. Ghiglieri V, Calabrese V, Calabresi P: **Alpha-Synuclein: From Early Synaptic Dysfunction to Neurodegeneration.** *Front Neurol* 2018, **9:**295.
23. Hass EW, Sorrentino ZA, Xia Y, Lloyd GM, Trojanowski JQ, Prokop S, Giasson BI: **Disease-, region- and cell type specific diversity of α-synuclein carboxy terminal truncations in synucleinopathies.** *Acta Neuropathologica Commun* 2021, **9:**146.
24. Lau A, So RWL, Lau HHC, Sang JC, Ruiz-Riquelme A, Fleck SC, Stuart E, Menon S, Visanji NP, Meisl G, et al: **α-Synuclein strains target distinct brain regions and cell types.** *Nat Neurosci* 2020, **23:**21-31.
25. Taguchi K, Watanabe Y, Tsujimura A, Tanaka M: **Brain region-dependent differential expression of alpha-synuclein.** *J Comp Neurol* 2015, **524:**1236-1258.
26. Chen L, Nagaraja C, Daniels S, Fisk ZA, Dvorak R, Meyerdirk L, Steiner JA, Galvis MLE, Henderson MX, Rousseaux MWC, et al: **Synaptic location is a determinant of the detrimental effects of α-Synuclein pathology to glutamatergic transmission in the basolateral amygdala.** *Elife* 2022, **11**.
27. Thakur P, Chiu WH, Roeper J, Goldberg JA: **α-SYNUCLEIN 2.0 – Moving towards Cell-Type Specific Pathophysiology.** *Neuroscience* 2019, **412:**248-256.
28. Turrigiano G: **Too Many Cooks? Intrinsic and Synaptic Homeostatic Mechanisms in Cortical Circuit Refinement.** *Annu Rev Neurosci* 2011, **34:**89-103.
29. Sorrentino ZA, Goodwin MS, Riffe CJ, Dhillon J-KS, Xia Y, Gorion K-M, Vijayaraghavan N, McFarland KN, Golbe LI, Yachnis AT, Giasson BI: **Unique α-synuclein pathology within**

821 **the amygdala in Lewy body dementia: implications for disease initiation and**
822 **progression.** *Acta Neuropathologica Commun* 2019, **7:**142.
823 30. Nelson PT, Abner EL, Patel E, Anderson S, Wilcock DM, Kryscio RJ, Eldik LJV, Jicha GA, Gal
824 Z, Nelson RS, et al: **The Amygdala as a Locus of Pathologic Misfolding in**
825 **Neurodegenerative Diseases.** *J Neuropathology Exp Neurology* 2017, **77:**2-20.
826 31. Flores-Cuadrado A, Ubeda-Bañon I, Saiz-Sanchez D, Martinez-Marcos A: **α-**
827 **Synucleinopathy in the Human Amygdala in Parkinson Disease: Differential**
828 **Vulnerability of Somatostatin- and Parvalbumin-Expressing Neurons.** *J Neuropathology*
829 *Exp Neurology* 2017, **76:**754-758.
830 32. Harding AJ, Stimson E, Henderson JM, Halliday GM: **Clinical correlates of selective**
831 **pathology in the amygdala of patients with Parkinson's disease.** *Brain J Neurology*
832 2002, **125:**2431-2445.
833 33. Hu X, Song X, Yuan Y, Li E, Liu J, Liu W, Liu Y: **Abnormal functional connectivity of the**
834 **amygdala is associated with depression in Parkinson's disease.** *Movement Disorders*
835 2015, **30:**238-244.
836 34. Thobois S, Prange S, Sgambato-Faure V, Tremblay L, Broussolle E: **Imaging the Etiology of**
837 **Apathy, Anxiety, and Depression in Parkinson's Disease: Implication for Treatment.**
838 *Curr Neurol Neurosci* 2017, **17:**76.
839 35. Bowers D, Miller K, Mikos A, Kirsch-Darrow L, Springer U, Fernandez H, Foote K, Okun M:
840 **Startling facts about emotion in Parkinson's disease: blunted reactivity to aversive**
841 **stimuli.** *Brain* 2006, **129:**3356-3365.
842 36. Yoshimura N, Kawamura M, Masaoka Y, Homma I: **The amygdala of patients with**
843 **Parkinson's disease is silent in response to fearful facial expressions.** *Neuroscience*
844 2005, **131:**523-534.
845 37. Volpicelli-Daley LA, Luk KC, Lee VMY: **Addition of exogenous α-synuclein preformed**
846 **fibrils to primary neuronal cultures to seed recruitment of endogenous α-synuclein to**
847 **Lewy body and Lewy neurite–like aggregates.** *Nat Protoc* 2014, **9:**2135-2146.
848 38. West MJ: **Stereological methods for estimating the total number of neurons and**
849 **synapses: issues of precision and bias.** *Trends Neurosci* 1999, **22:**51-61.
850 39. Stoyka LE, Arrant AE, Thrasher DR, Russell DL, Freire J, Mahoney CL, Narayanan A, Dib
851 AG, Standaert DG, Volpicelli-Daley LA: **Behavioral defects associated with amygdala and**
852 **cortical dysfunction in mice with seeded α-synuclein inclusions.** *Neurobiol Dis*
853 2019**:**104708.
854 40. Burtscher J, Copin J-C, Rodrigues J, Kumar ST, Chiki A, Suduiraut M-IGd, Sandi C, Lashuel
855 HA: **Chronic corticosterone aggravates behavioural and neuronal symptomatology in a**
856 **mouse model of alpha-synuclein pathology.** *Neurobiol Aging* 2019, **83:**11-20.
857 41. Henderson MX, Cornblath EJ, Darwich A, Zhang B, Brown H, Gathagan RJ, Sandler RM,
858 Bassett DS, Trojanowski JQ, Lee VMY: **Spread of α-synuclein pathology through the**
859 **brain connectome is modulated by selective vulnerability and predicted by network**
860 **analysis.** *Nat Neurosci* 2019, **22:**1248-1257.
861 42. Osterberg Valerie R, Spinelli Kateri J, Weston Leah J, Luk Kelvin C, Woltjer Randall L, Unni
862 Vivek K: **Progressive Aggregation of Alpha-Synuclein and Selective Degeneration of**
863 **Lewy Inclusion-Bearing Neurons in a Mouse Model of Parkinsonism.** *Cell Reports* 2015,
864 **10:**1252-1260.

865 43. Volpicelli-Daley LA: **Effects of α-synuclein on axonal transport.** *Neurobiol Dis* 2017,
866 **105:**321-327.
867 44. Huang WC, Zucca A, Levy J, Page DT: **Social Behavior Is Modulated by Valence-Encoding**
868 **mPFC-Amygdala Sub-circuitry.** *Cell Rep* 2020, **32:**107899.
869 45. McGarry LM, Carter AG: **Prefrontal Cortex Drives Distinct Projection Neurons in the**
870 **Basolateral Amygdala.** *Cell Reports* 2017, **21:**1426-1433.
871 46. Likhtik E, Stujenske JM, Topiwala MA, Harris AZ, Gordon JA: **Prefrontal entrainment of**
872 **amygdala activity signals safety in learned fear and innate anxiety.** *Nat Neurosci* 2014,
873 **17:**106-113.
874 47. Xu S, Jiang M, Liu X, Sun Y, Yang L, Yang Q, Bai Z: **Neural Circuits for Social Interactions:**
875 **From Microcircuits to Input-Output Circuits.** *Front Neural Circuits* 2021, **15:**768294.
876 48. Felix-Ortiz AC, Tye KM: **Amygdala Inputs to the Ventral Hippocampus Bidirectionally**
877 **Modulate Social Behavior.** *J Neurosci* 2014, **34:**586-595.
878 49. Good CH, Hoffman AF, Hoffer BJ, Chefer VI, Shippenberg TS, Bäckman CM, Larsson N-G,
879 Olson L, Gellhaar S, Galter D, Lupica CR: **Impaired nigrostriatal function precedes**
880 **behavioral deficits in a genetic mitochondrial model of Parkinson's disease.** *Faseb J*
881 2011, **25:**1333-1344.
882 50. O'Keeffe GW, Sullivan AM: **Evidence for dopaminergic axonal degeneration as an early**
883 **pathological process in Parkinson's disease.** *Parkinsonism Relat Disord* 2018, **56:**9-15.
884 51. Froula JM, Henderson BW, Gonzalez JC, Vaden JH, McLean JW, Wu Y, Banumurthy G,
885 Overstreet-Wadiche L, Herskowitz JH, Volpicelli-Daley LA: **α-Synuclein fibril-induced**
886 **paradoxical structural and functional defects in hippocampal neurons.** *Acta*
887 *Neuropathologica Commun* 2018, **6:**35.
888 52. Subramaniam M, Althof D, Gispert S, Schwenk J, Auburger G, Kulik A, Fakler B, Roeper J:
889 **Mutant α-Synuclein Enhances Firing Frequencies in Dopamine Substantia Nigra**
890 **Neurons by Oxidative Impairment of A-Type Potassium Channels.** *J Neurosci* 2014,
891 **34:**13586-13599.
892 53. Guatteo E, Rizzo FR, Federici M, Cordella A, Ledonne A, Latini L, Nobili A, Viscomi MT,
893 Biamonte F, Landrock KK, et al: **Functional alterations of the dopaminergic and**
894 **glutamatergic systems in spontaneous α-synuclein overexpressing rats.** *Exp Neurol*
895 2017, **287:**21-33.
896 54. Bian WJ, Brewer CL, Kauer JA, de Lecea L: **Adolescent sleep shapes social novelty**
897 **preference in mice.** *Nat Neurosci* 2022, **25:**912-923.
898 55. Gonzalez LE, Andrews N, File SE: **5-HT1A and benzodiazepine receptors in the**
899 **basolateral amygdala modulate anxiety in the social interaction test, but not in the**
900 **elevated plus-maze.** *Brain Res* 1996, **732:**145-153.
901 56. Geertsma HM, Fisk ZA, Sauline L, Prigent A, Kurgat K, Callaghan SM, a S-PDC, Henderson
902 MX, Rousseaux MWC: **A topographical atlas of alpha-synuclein dosage and cell type-**
903 **specific expression in adult mouse brain and peripheral organs.** *NPJ Parkinsons Dis*
904 2024, **10:**65.
905 57. Chatterjee D, Sanchez DS, Quansah E, Rey NL, George S, Becker K, Madaj Z, Steiner JA,
906 Ma J, Galvis MLE, et al: **Loss of One Engrailed1 Allele Enhances Induced α-**
907 **Synucleinopathy.** *J Park Dis* 2019, **9:**315-326.

58. Shin R-M, Tully K, Li Y, Cho J-H, Higuchi M, Suhara T, Bolshakov VY: **Hierarchical order of coexisting pre- and postsynaptic forms of long-term potentiation at synapses in amygdala.** *Proceedings of the National Academy of Sciences* 2010, **107:**19073-19078.
59. Siguròsson T, Sigurdsson T, Cain CK, Doyère V, LeDoux JE: **Asymmetries in long-term and short-term plasticity at thalamic and cortical inputs to the amygdala in vivo.** *Eur J Neurosci* 2010, **31:**250-262.